HHS Public Access

Author manuscript

Nature. Author manuscript; available in PMC 2021 September 17.

Expansible residence decentralizes immune homeostasis

Sathi Wijeyesinghe[1], **Lalit K. Beura**[1,3], **Mark J. Pierson**[1], **J. Michael Stolley**[1], **Omar A. Adam**[1], **Roland Ruscher**[2,4], **Elizabeth M. Steinert**[1], **Pamela C. Rosato**[1,5], **Vaiva Vezys**[1], **David Masopust**[1,*]

[1]Center for Immunology and Department of Microbiology & Immunology, University of Minnesota, Minneapolis, MN, USA.

[2]Center for Immunology and Department of Laboratory Medicine & Pathology, University of Minnesota, Minneapolis, MN, USA.

[3]Present address: Department of Molecular Microbiology and Immunology, Brown University, Providence, RI, USA.

[4]Present address: Centre for Molecular Therapeutics, Australian Institute of Tropical Health & Medicine, James Cook University, Cairns, QLD, Australia.

[5]Present address: Department of Microbiology and Immunology, The Geisel School of Medicine at Dartmouth, Lebanon, NH, USA.

Abstract

Metazoans relegate specific tasks to dedicated organs that are established early in development, occupy discrete anatomic locations, and typically remain fixed in size. The adult immune system arises from a centralized hematopoietic niche that maintains self-renewing potential[1,2], and upon maturation, becomes distributed throughout the body to monitor environmental perturbations, regulate tissue homeostasis, and mediate organism-wide defense. This study examines how immunity is integrated within adult mouse tissues while addressing issues of durability, expansibility, and contribution to organ cellularity. Focusing on antiviral T cell immunity, we observe durable maintenance of resident memory T cells (T_{RM}) up to 450 days after infection. Once established, resident T cells did not require the T cell receptor for survival or retention of a poised effector-like state. While resident memory indefinitely dominated most mucosal organs, surgical separation of parabiotic mice unexpectedly revealed a tissue-resident provenance for bloodborne effector memory T cells, and circulating memory slowly made substantial contributions to tissue immunity in some organs. Following additional microbial experiences via serial immunizations or pet shop mice co-housing, for most tissues we find tissue pliancy allows for the accretion of tissue-resident memory, without axiomatic erosion of preexisting antiviral T

[*]**Correspondence and requests for materials** should be addressed to D.M. masopust@umn.edu.

Author contributions

S.W., L.K.B., M.J.P., J.M.S., O.A.A., R.R., E.M.S, and P.C.R. performed the experiments; S.W., V.V., and D.M. designed the experiments and wrote the manuscript.

Competing interests

The authors declare no competing interests.

cell immunity. Extending these findings, we demonstrate tissue residence and organ pliancy are generalizable aspects underlying the homeostasis of innate and adaptive immunity. The immune system-at-large grows commensurate to microbial experience reaching up to 25% of visceral organ cellularity. Regardless of location, many white blood cell populations adopted a tissue residency program within nonlymphoid organs. Thus, residence, rather than renewal or recirculation, typifies nonlymphoid immune surveillance, and organs serve as a pliant storage reservoir that can accommodate the continuous expansion of the cellular immune system throughout life. While hematopoiesis ('to make blood') restores certain elements of the immune system, in parallel, nonlymphoid organs sustain an accrual of durable tissue-autonomous cellular immunity, resulting in the progressive decentralization of organismal immune homeostasis.

T_{RM} longevity is TCR-independent

Most immune cells function locally[3,4]. For example, T cells require contact with neighboring cells to sense and eliminate infections or tumors[5-7]. To systematically evaluate the longevity of memory T cells in different locations, we transferred CD45.1$^+$ or Thy1.1$^+$ P14 CD8$^+$ T cells into naive female C57Bl/6J mice followed by LCMV Armstrong infection (referred to as P14 immune chimeras). Nonlymphoid tissues are surveyed by T_{RM}, which are vulnerable to apoptosis upon tissue digestion making enumeration by this method inadequate[8,9]. To mitigate this issue, we visually enumerated P14 CD8$^+$ T cells by quantitative immunofluorescent microscopy (QIM) between five and 450 days after LCMV infection in tissues of 80-96 mice (Fig. 1a-e). The response to LCMV peaked within 5-9 days before contracting. A stable population of memory was established in the lymph node by 16 days after infection. We found considerable variation in the durability of nonlymphoid T_{RM}, which were stable in salivary gland, decayed modestly in the small intestine (best modeled by biphasic decay), and underwent continued attrition in the uterus. T_{RM} attrition was particularly noted within uterine endometrium, which underwent vacuolation and glandular atrophy in aged mice (Extended Data Fig. 1a-c), coinciding with infertility. Aging was also associated with the development of prominent peripheral node addressin-expressing tertiary lymphoid organs in salivary glands (excluded from T_{RM} enumeration in Fig. 1c; Extended Data Fig. 1d, e). These data indicate that memory CD8$^+$ T cell longevity varies by location, but in some compartments can persist indefinitely.

Naïve and central memory (T_{CM}) T cells recirculate between blood and lymph nodes. Naive T cells depend on constitutive T cell receptor (TCR) signaling for survival, while T_{CM} do not[10]. Unlike T_{CM}, T_{RM} share many properties with T cells undergoing recent TCR stimulation[11,12]. To test whether T_{RM} persistence depends on the TCR, we took advantage of UBC-CreER^{T2} x TCR$\alpha^{fl/fl}$ mice (hereon referred to as TCR$\alpha^{fl/fl}$), so that we could genetically ablate the TCR by tamoxifen treatment in established memory T cells (see Extended Fig. 2, 3 and methods). WT Thy1.1$^+$ and TCR$\alpha^{fl/fl}$ Thy1.1$^-$ cells were compared within the same mice and TCR ablation was confirmed by staining for TCRβ and a failure to produce cytokines in response to ex vivo peptide stimulation (Fig. 1f, g, Extended Data Fig. 2a-e, and Extended Data Fig. 3a-c). No significant difference was observed between the longevity of WT and TCR-ablated T_{RM} in all tissues examined, nor was expression of CD69 and CD103 reduced on TCR-ablated memory T cells (Fig. 1h-j, Extended Data Fig. 2f-h,

and Extended Data Fig. 3d). Thus, $CD8^+$ T_{RM} are not maintained by persistent viral antigen, self-peptide–MHC I complexes, or cross-reactivity with microbial TCR ligands.

Durability of T_{RM} organ surveillance

The defining characteristic of T_{RM} is the absence of migration. However, migration experiments are typically short-term, raising the question of whether T_{RM} populations are gradually replenished by T_{CM}[13] or slowly recirculating[14-16]. To address this issue, we generated mice harboring either $CD45.1^+$ or $Thy1.1^+$ memory P14 $CD8^+$ T cells by LCMV infection. 30 days later, we conjoined mice by parabiosis, which resulted in equilibration of circulating memory P14 $CD8^+$ T cells in the blood of paired mice. Parabionts were separated 30 days after conjoining, which allowed for prolonged monitoring of residence (Fig. 1k). 260 days after LCMV infection (200 days after separation), memory T cells were of host origin in most nonlymphoid tissues, indicating that T_{RM} autonomously dominate immunosurveillance for the lifespan of the mouse (Fig. 1l). Organized lymphoid structures, including tertiary lymphoid organs in salivary gland and Peyer's patches in small intestine, were surveyed by both recirculating and resident memory T cells. However, extravascular memory T cells in the lung parenchyma demonstrated near-complete equilibration regardless of CD69 expression (Fig. 1l and Extended Data Fig. 4a, b). Although T_{RM} seed the lung shortly after infection, these data indicate that long-term pulmonary surveillance may depend on circulating memory T cells that enter the tissue, which has ramifications for the durability of T cell-dependent protection against respiratory infections[17,18]. Circulating memory T cells also eventually made substantial contributions to the maintenance of memory in liver and kidney (Fig. 1l). While these observations offer support for a centralized source for nonlymphoid memory in certain locations[13], for most tissues, residence is responsible for long-term surveillance after clearance of primary infections in mice housed under specific pathogen free (SPF) laboratory conditions.

T_{RM} gradually originate memory in blood

Primary infections induce $CD62L^-/KLRG1^-$ long-lived effector memory T cells (T_{EM}) that patrol blood without entering lymph nodes. After surgical separation, we unexpectedly observed a gradual disequilibrium in blood, in favor of host-derived P14 $CD8^+$ T cells (Fig. 1l-n and Extended Data Fig. 5a, b). These data indicate that T cells that failed to equilibrate during parabiosis (i.e., T_{RM}) slowly join the blood circulation. Over time, these ex-T_{RM} came to comprise between 15-30% of all memory P14 T cells in peripheral blood (Extended Data Fig. 5a, b) and were significantly enriched within the $KLRG1^-$ T_{EM} subset (Fig. 1m, n). Additional profiling revealed that expression of the CD43 glycoform, recognized by the 1B11 antibody clone, further distinguished ex-T_{RM}, consistent with expression of this glycoform on tissue resident memory cells (Fig. 1o, Extended Data Fig. 5c, and Extended Data Fig. 6a, b). Thus, while T_{RM} wane in some nonlymphoid tissues, they contemporaneously give rise to bloodborne T_{EM}.

The T_{RM} niche is expansible

Cell populations are often numerically fixed in size by cell-extrinsic regulators[19]. Cytokine abundance (e.g., IL-15), metabolite availability, and constitutive TCR signaling all function to restrict T cell abundance in blood, yet these factors do not axiomatically control T cell survival in tissues[20-22]. We hypothesized that the resident memory pool may circumvent the numerical constraints imposed on bloodborne T cells. We previously employed a reductionist approach to test whether the circulating memory $CD8^+$ T cell population in blood, spleen, and lymph nodes was expansible or rigidly defined[23], and apply that approach here for the analysis of nonlymphoid tissues dominated by T_{RM} (Fig. 1). P14 $CD8^+$ T cell memory was established by LCMV infection (as in Fig. 1a-e). Sixty days after LCMV infection, we initiated a potent heterologous prime-boost (HPB) vaccination regimen that established a large, broadly distributed memory $CD8^+$ T cell population specific for the immunodominant nucleoprotein (N) epitope of vesicular stomatitis virus (VSV) (Fig. 2a, b). Concomitant with the expansion of N-specific memory T cells, there was a reduction in the relative frequency of preexisting P14 $CD8^+$ T cells as a fraction of total $CD8^+$ T cells (Fig. 2c). However, enumeration of P14 $CD8^+$ T cells via QIM demonstrated that T_{RM} were numerically preserved (Fig. 2d). In contrast to a previous study[24], new immunizations did not compromise the capacity of preexisting memory $CD8^+$ T cells to produce antiviral cytokines (Fig. 2e and Extended Data Fig. 7a). These data indicate that the immunological ‘space’ or carrying capacity for T_{RM} is malleable, allowing for the coexistence of established immunity and de novo immune responses.

To assess whether preexisting T_{RM} were also durably maintained following diverse physiologic microbial exposure, we took advantage of a recently developed co-housing model that effects pronounced changes in innate and adaptive immunity. Co-housing SPF mice with pet shop mice results in transmission of bacteria, viruses, fungi, and helminths, and induces extensive immune activation and adoption of a more human-like immune system[25]. Sixty days after LCMV, P14 chimeras were co-housed with pet shop mice for two months (Fig. 2f, g). In most tissues, we observed little attrition of P14 $CD8^+$ T cells, indicating that circulating and resident memory $CD8^+$ T cells can persist in the face of substantial microbial exposure (Fig. 2h, i). Of note, the resident property of memory P14 $CD8^+$ T cells in tissues was also preserved in mice subject to co-housing with pet shop mice (Fig. 2j) suggesting that residence itself is not an artifact of artificially clean mouse husbandry. Small intestine T_{RM} constituted an exception and were nearly six-fold less abundant following co-housing. Intestinal T_{RM} attrition may reflect saturation of anatomic space, heightened damage-associated molecular patterns (DAMPs) that induce cellular toxicity[9], or microbiome alterations that modulate local survival cues. In two alternative infection models that generate lung- or skin-resident memory $CD8^+$ T cells respectively, preexisting memory was preserved following co-housing (Extended Data Fig. 8a-g). Thus, in most tissues, HPB vaccination or physiological microbial exposure did not induce erosion of T_{RM}, but instead tissues accommodated more resident cells.

Immune system is expansible tissue component

Homeostasis balances cellular self-renewal with cell death and maintains organ size in adult organisms. This process preserves organ function while preventing cancer. The expansible nature of the T cell compartment raised questions about whether the immune system *in toto* adheres to a fixed size or exhibits pliancy in proportion to microbial experience. Indeed, co-housing induced a durable increase in nearly all leukocyte cell types in blood and persistent enlargement of lymph nodes and spleen (Fig. 3a-c). Both memory $CD4^+$ and $CD8^+$ T cells increased following co-housing and even so-called 'innate' populations of the immune system demonstrated an 'adaptive' ability to durably expand in magnitude (Fig. 3a-c and Extended Data Fig. 9a, b). Extensive QIM analysis revealed that 5-20% of most nonlymphoid tissues of SPF mice were composed of white blood cells. However, the frequency of immune cells was significantly and durably expanded after co-housing, indicating that the immune system occupies a considerable fraction of visceral and mucosal organs, is flexible in size, and is capable of long-lived adaptation in relation to microbial exposure (Fig. 3d, e).

Residency typifies tissue immunity

Memory T cells achieve durable immune surveillance of the entire organism through prolonged residence in most nonlymphoid tissues (Fig. 1). Tissue residency has been appreciated for several immune cell types primarily in immunologically naïve or single-infection mouse models[26,27]. We asked whether residence is a common mechanism employed by the immune system at-large to achieve broad immunological surveillance by performing parabiosis surgery of co-housed B6 mice that have diverse microbial experience (Extended Data Fig. 10a). Leukocytes (distinguished by CD45) equilibrated completely within peripheral blood of parabiotic mice (Extended Data Fig. 10b), but tissue-resident immune populations occupied and often dominated most mouse organs (Fig. 4a). Over one month, many $CD4^+$ and $CD8^+$ T cells of the adaptive immune system, as well as macrophages, innate lymphoid cells, and NK cells of the innate immune system stably occupied nonlymphoid tissues (Fig. 4b and Extended Data Fig. 10c-f). Consistent with their rapid turnover, granulocytes in tissues relied on continuous replenishment from blood (Fig. 4b and Extended Data Fig. 10g). B cells, which differentiate into the antibody secreting cells of the immune system, largely equilibrated between parabionts (Fig. 4b and Extended Data Fig. 10h). Overall, residence was a shared feature exhibited by many adaptive and innate immune cell types in mice exposed to diverse microbes.

Conclusion

The immune system has defied classification as a commonly recognized organ system, but is partially captured by the skeletal system (includes bone marrow), the cardiovascular system (includes blood cells), and the lymphatic system (includes secondary lymphoid organs)[28,29]. This framework excludes many immune cells in the body, particularly those most responsible for regional immune surveillance and effector functions. Our study generalizes two features of immunity outside of dedicated lymphoid organs: 1) most immune cells stably reside in, rather than recirculate through, tissues and 2) the size of the immune system

durably adapts to microbial experience to accommodate additional cells. While parenchymal cell populations are numerically constrained to maintain organ homeostasis, the adaptive flexibility of the immune system allows leukocytes to comprise a considerable fraction of the body – up to a quarter of visceral organs in microbially experienced mice. Analyses limited to blood and lymphoid organs have emphasized the renewable and migratory aspects of the immune system[30-33]. Initially focused reductively on T cells, we show that resident T cell immunity can autonomously endure over time, without displacement by subsequent inflammation, infection, or competition for a fixed immunological niche. Given that most infections and tumors develop in nonlymphoid organs, these are relevant findings for immunization strategies that seek to harness T cell immunity[34,35]. In contrast to expectations, we observed that most long-lived bloodborne T_{EM} are ex-T_{RM} after a primary infection (Fig. 1), and recent reports indicate that reactivated T_{RM} likely contribute even further to circulating memory populations[36,37]. The phenomenon of expansible residence observed for T cells extended to most immune cell populations. While immune responses develop in centralized sites, our data indicate that nonlymphoid organs provide a flexible reservoir for the long-term preservation of adaptive and innate immunity. Given these findings, it may be reasonable to conceptualize the immune system at-large as its own organ system; albeit one comprised of a diverse network of motile sensory cells that are durably integrated throughout the entire body, and permissive to significant plasticity in cell number, composition, and distribution.

Methods

Mice

Female SPF C57BL/6J (CD45.2$_+$ B6) and B6.SJL-Ptprc^{a}Pepc^b/BoyJ (CD45.1$^+$ B6) mice 6-8 weeks of age were purchased from The Jackson Laboratory. For co-housing experiments, female SPF CD45.2$^+$ and CD45.1$^+$ B6 mice 6-8 weeks of age were purchased from Charles River Laboratories. Female pet shop mice (age not provided by vendor) were purchased from various pet shops in the greater Minneapolis-St. Paul metropolitan area. Co-housing of SPF mice with sex-matched pet shop mice was performed as described[19] within the University of Minnesota BSL-3 facility. The following housing conditions were regulated: ambient temperature (20.0-23.3°C), humidity (30-70%), light/dark cycling (14 hours on/ 10 hours off). TCR$\alpha^{fl/fl}$ mice[38] were fully backcrossed to UBC-CreER^{T2} mice[39] (JAX stock no. 007001) to generate UBC-CreER^{T2} TCR$\alpha^{fl/fl}$ mice (provided by K. Hogquist). Male and female UBC-CreER^{T2} TCR$\alpha^{fl/fl}$ mice 6-10 weeks of age were used in tandem with age- and sex-matched Thy1.1$^+$ B6 mice. CD45.1$^+$ sex-matched mice 6-12 weeks of age were used as recipient mice. P14 CD8$^+$ T cell transgenic, Thy1.1$^+$ B6, and CD45.1$^+$ B6 mouse strains were maintained in house. In experiments with multiple groups, littermates of the same sex were randomly assigned to experimental groups. All mice were used in accordance with guidelines established by the Institutional Animal Care and Use Committee at the University of Minnesota.

Adoptive transfers and infections

P14 immune chimeras were generated by intravenous (i.v.) adoptive transfer of 5 x 10^4 P14 CD8$^+$ splenocytes into naive female B6 mice and infection with 2 x 10^5 plaque-forming

units (PFU) of the Armstrong strain of lymphocytic choriomeningitis virus (LCMV) via intraperitoneal (i.p.) injection on the subsequent day. Alternatively, P14 immune chimeras were generated by i.v. adoptive transfer of 5 x 10^4 P14 $CD8^+$ splenocytes into naive female B6 mice and intranasal infection with 500 PFU PR8-gp33 recombinant influenza virus (provided by R. Langlois) on the subsequent day. OT-1 immune chimeras were generated by i.v. transfer of 5 x 10^4 OT-1 $CD8^+$ splenocytes into naïve female B6 mice and infection with 10^6 PFU vesicular stomatitis virus (VSV)-OVA the following day. For experiments using $TCR\alpha^{fl/fl}$ mice, $TCR\alpha^{fl/fl}$ mice and WT $Thy1.1^+$ B6 mice were intraperitoneally infected with 2 x 10^5 PFU of LCMV. After 30 days, 10^7 lymphocytes, isolated from secondary lymphoid organs, were i.v. transferred into naive $CD45.1^+$ B6 mice. On the subsequent day, $CD45.1^+$ recipients were i.p. infected with 10^6 PFU of LCMV. To generate primary polyclonal memory with $TCR\alpha^{fl/fl}$ mice, naïve $TCR\alpha^{fl/fl}$ mice and WT $Thy1.1^+$ B6 mice were sacrificed and $CD8^+$ T cells were enriched from secondary lymphoid organs via negative selection per manufacturer's protocol (Stem Cell Technologies). A total of 2 x 10^6 enriched cells were stimulated in flat-bottom 12-well plates with anti-CD3ε (clone 145-2C11, 10 μg/mL; Bio X Cell) and rB7-1/Fc chimeric protein (0.8 μg/mL; R&D Systems) immobilized on the surface in the presence of 5 U/mL IL-2 (R&D Systems) with 10 ng/mL murine rIL-12 (R&D Systems) as described[40]. After 3 days of in vitro activation, 10^7 $CD8^+$ T cells isolated from $TCR\alpha^{fl/fl}$ mice and WT $Thy1.1^+$ B6 mice were i.v. co-transferred into naïve $CD45.1^+$ B6 mice. For heterologous prime boost immunization, three viruses were administered by i.v. injection at 30-day intervals in the following order, as described[23]: 1°: 10^6 PFU of VSV, New Jersey serotype, 2°: 2 x 10^6 PFU of recombinant vaccinia expressing the VSV nucleoprotein, 3°: 10^7 PFU of VSV, Indiana serotype.

Quantitative immunofluorescence microscopy

Harvested murine tissues were fixed in 2% paraformaldehyde for 2 hours, followed by overnight cryoprotection in 30% sucrose solution at 4°C. Sucrose-treated tissue was embedded in optimal cutting temperature (OCT) compound and frozen in a chilled isopentane bath. Alternatively, harvested murine tissues were directly embedded in OCT compound and snap-frozen in a chilled isopentane bath. Studies of the salivary gland focused exclusively on the submandibular gland. Frozen tissue blocks were sectioned at 7-μm in a Leica cryostat. Sections were stained with primary and secondary antibodies, counterstained with either 4′,6-diamidino-2-phenylindole (DAPI) or SYTOX Green to detect nuclei, and immunofluorescence microscopy was performed using a Leica DM6000 B microscope. Monoclonal anti-mouse antibodies used at a 1:100 dilution unless otherwise noted were: CD8α (53-6.7), CD8β (YTS156.7.7), CD45 (30-F11), CD45.1 (A20), Thy1.1 (OX-7) (1:1000), B220 (RA3-6B2), EpCAM (G8.8) (1:500), PNAd (MECA-79) from BioLegend. Polyclonal goat anti-mouse collagen type IV antibody (1:200) from MilliporeSigma and secondary bovine anti-goat IgG (H+L) antibody (1:300) from Jackson ImmunoResearch were used. Images were processed using FIJI software[41] and cell enumeration was performed manually as previously described[8] or using ImageJ scripts developed in house.

Leukocyte isolation and phenotyping of cells

An intravascular staining method was used to discriminate between cells within the vasculature and those within the parenchyma of tissues. Three minutes prior to sacrifice, mice were intravenously injected with either 3 μg of biotinylated- or fluorophore-conjugated CD8α (53-6.7) antibody or 2 μg of fluorophore-conjugated CD45 (30-F11) antibody[42]. Tissues were harvested and leukocytes isolated as previously described[8]. Studies of the salivary gland focused exclusively on the submandibular gland. Isolated leukocytes were surface-stained with monoclonal anti-mouse monoclonal antibodies at a 1:100 dilution unless otherwise noted: CD4 (GK1.5), CD5 (53-7.3), CD8α (53-6.7), CD8β (53-5.8), CD11c (N418), CD43 (1B11), CD44 (IM7), CD45 (30-F11), CD45.1 (A20), CD45.2 (104), CD62L (MEL-14), CD64 (X54-5/7.1), CD69 (H1.2F3), CD103 (2E7), Thy1.1 (OX-7) (1:250), B220 (RA3-6B2), F4/80 (BM8), Ly6C (HK1.4) (1:400), Ly6G (1A8), NKp46 (29A1.4), PD-1 (29F.1A12), CX3CR1 (SA011F11), CXCR3 (CXCR3-173) from BioLegend; CD11b (M1/70), CD19 (1D3), NK1.1 (PK136), Siglec-F (E50-2440), TCF-1 (S33-966) (1:50) from BD; CD3ε (145-2C11), CD127 (A7R34), KLRG1 (2F1), TCRβ (H57-597) from Tonbo Biosciences. Cell viability was determined using Ghost Dye Violet 510 or Ghost Dye Red 780 (Tonbo Biosciences) (1:300). To identify VSV nucleoprotein-specific $CD8^+$ T cells, leukocytes were stained with H-$2K^b$/N (MHC class I tetramer) (1:200), conjugated to PE. To identify gp33-specific $CD8^+$ T cells, leukocytes were stained with H-$2D^b$/N (MHC class I tetramer) (1:200), conjugated to APC. Staining for intracellular transcription factors and proteins was performed using a transcription factor staining buffer kit (Tonbo Biosciences) with monoclonal anti-mouse antibodies: T-bet (4B10) from BioLegend; Eomes (Dan11mag), Foxp3 (FJK-16s), Gata-3 (TWAJ), Ki67 (SolA15) (1:400), Rorγt (B2D) from ThermoFisher Scientific. The stained samples were acquired using LSRII or LSR Fortessa flow cytometers (BD) and analyzed with FlowJo software (BD). Neutrophils were distinguished by expression of CD11b and Ly6G. Eosinophils were identified by Siglec-F expression. Innate lymphoid, natural killer, B cell, and monocyte/macrophage populations were distinguished after excluding lineage-positive cells using combinations of CD3, CD5, CD19, B220, and Ly6G and then using recommended lineage defining-markers as described[43,44]. Monocytes were further subdivided into classical and patrolling populations on the basis of Ly6C expression. Lung macrophages were subdivided into alveolar and interstitial populations on the basis of Siglec-F and CD11b expression.

Parabiosis and separation surgeries

Parabiosis and separation surgeries were performed with age-matched female mice as described[45] with some modifications. For surgeries, anesthesia to full muscle relaxation was achieved using avertin (250 mg/kg) by i.p. injection and surgical site preparation included betadine application to surgical site in a gradually enlarging circular pattern. For parabiosis, corresponding lateral aspects of mice were thoroughly shaved with electric clippers from ~1 cm superior to the shoulder and ~1 cm inferior to the hip. Excess hair was wiped off with alcohol prep pads. Following surgical site preparation, matching skin incisions were made ~0.5 cm superior to the shoulder and ~0.5 cm inferior to the hip. Subcutaneous fascia was bluntly dissected to create ~0.5 cm of free skin. Dorsal and ventral skins of adjacent mice were approximated by interrupted horizontal mattress stitches with 3-0 Prolene suture and overlying surgical wound clips. To separate parabiotic mice, preexisting suture and wound

clips were removed. Excess hair was shaved and wiped off with alcohol prep pads. After surgical site preparation, a longitudinal incision was made with sharp scissors lateral to the initially conjoined skin. Newly formed fascia was gently detached with a pair of curved forceps. The superior and inferior aspects of the skin of each mouse were then approximated by running stitch with a single 4-0 Vicryl suture. For analgesic treatment, mice received preoperative subcutaneous buprenorphine (2mg/kg) and postoperative subcutaneous bupivacaine (2mg/kg) and carprofen (5mg/kg). Mice were kept on heating pads during and after surgery and their recovery was monitored continuously.

Tamoxifen administration

Tamoxifen was dissolved in corn oil at 37°C with shaking overnight to a working concentration of 20 mg/ml. Working stocks were freshly prepared for each experiment. For $CreER^{T2}$ induction, tamoxifen was administered to mice i.p at a dose of 75 mg/kg every 24 hours over five consecutive days.

In vitro stimulation assays

Isolated lymphocytes were incubated at 37°C for 4 hours in stimulation media with or without gp_{33-41} peptide (0.2 μg/mL) or phorbol myristate acetate (PMA) and ionomycin (Cell stimulation cocktail, ThermoFisher Scientific). Stimulation media consisted of RPMI 1640, 10% FCS, 2 mM L-glutamine, 100 U/ml penicillin, 100 mg/ml streptomycin, 50 mM 2-mercaptoethanol, and brefeldin A (GolgiPlug, BD). Intracellular staining for cytokines was performed using the Cytofix/Cytoperm kit (per manufacturer's directions, BD) with anti-mouse antibodies: IFN-γ (XMG1.2) from BioLegend and TNF-α (MP6-XT22) from ThermoFisher Scientific.

Quantification and Statistical Analysis

Specific statistical tests, sample size (n), and p-values can be found in figure legends. Individual data points represent biological replicates. All statistical tests were two-tailed and generally, non-parametric tests were used to test for significance (Mann-Whitney U test for unpaired samples, Wilcoxon matched-pairs signed rank test for paired samples). All statistical analysis was done using Prism (GraphPad). For all experiments, a p-value < 0.05 was considered significant. Mean and standard error of the mean are used to represent the center and dispersion, unless otherwise stated. Nonlinear regression analysis using Prism (GraphPad) was used to model memory T cell population kinetics data, using data points between 30 and 450 days post infection. Model constraints imposed that decay plateau = 0 and a positive rate constant. An exponential decay model was fit to tissue populations if $R^2 > 0$. Either one or two-phase exponential decay models were selected after comparison using extra sum-of-squares F test and the Akaike information criterion (AIC).

Data availability

The data that support the findings of this study are available from the corresponding author upon reasonable request.

Code availability

ImageJ scripts developed for cell enumeration are available at http://github.com/wijey001/count.

Extended Data

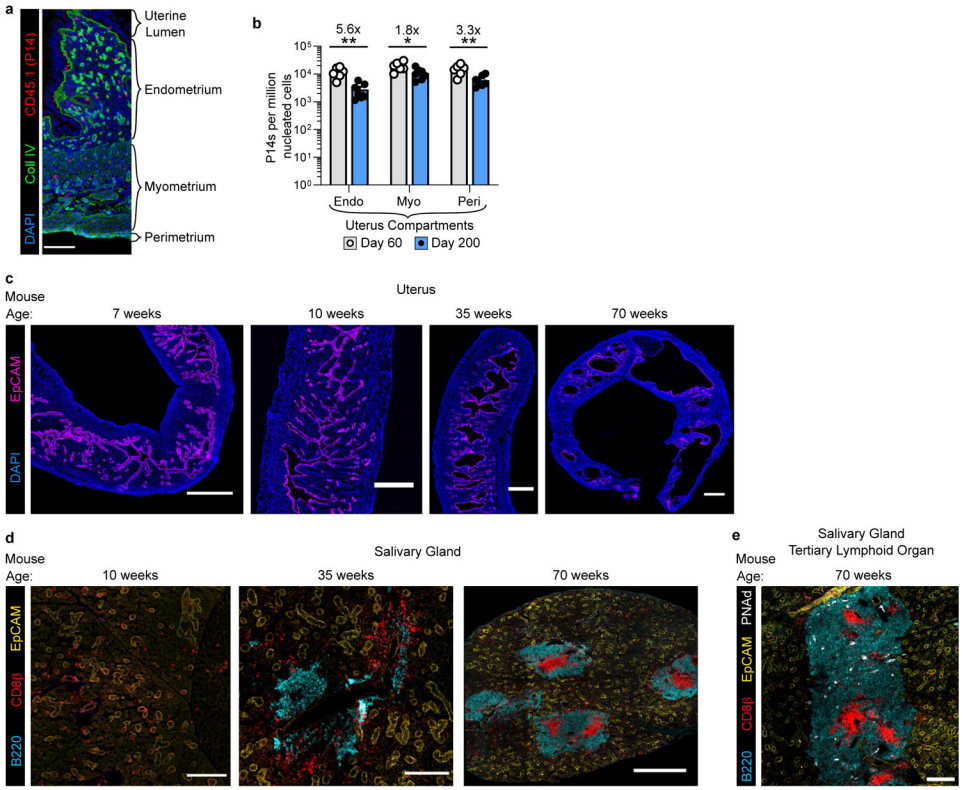

Extended Data Fig. 1. Compartmentalized decay of uterine T cells concomitant with morphological changes in tissue architecture over time.

a, Representative immunofluorescence of uterine tissue. **b,** The frequency of P14 memory $CD8^+$ T cells in uterine compartments was assessed by quantitative immunofluorescent microscopy at day 60 ($n = 6$ mice) and day 200 ($n = 7$ mice) after LCMV infection in one experiment. **c,** Representative immunofluorescence images of mouse uterine tissue at various ages demonstrating endometrial vacuolations in older mice . **d, e,** Representative immunofluorescence images of mouse salivary gland at various timepoints demonstrating emergence of salivary gland tertiary lymphoid organs in older mice (**d**) and expression of peripheral node addressin (PNAd) (**e**). Morphology representative of $n > 12$ mice, PNAd staining representative of $n = 5$ mice (**c**-**e**). Coll IV, collagen type IV. 100 μm scale bar (**a**), 500 μm scale bars (**c**), 200 μm scale bars (10/35 weeks) and 500 μm scale bar (70 weeks) (**d**), 200 μM scale bar (**e**). Statistical significance was determined by two-tailed Mann-Whitney U test (**b**) where $*p = 0.0221$, $**p = 0.0023$ (endometrium) or $**p = 0.0082$ (perimetrium). Data are presented as mean values +/− SEM.

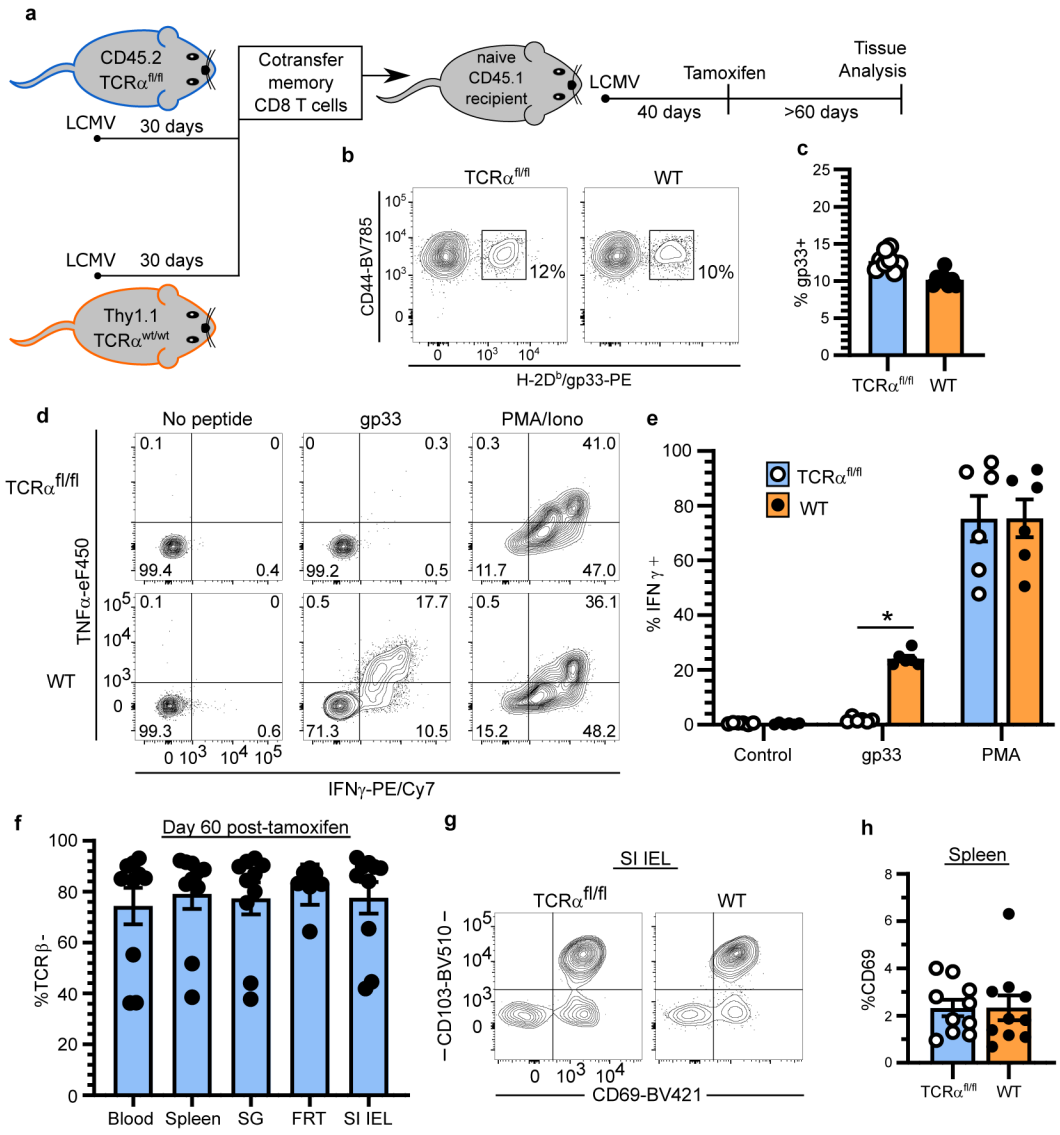

Extended Data Fig. 2. Selective TCR ablation using TCRα$^{fl/fl}$ mice reveals TCR-independent homeostasis of T_{RM}.

a, Experimental model. Thy1.1^{-}/CD45.2^{+} UBC-CreER^{T2} TCRα$^{fl/fl}$ mice (TCRα$^{fl/fl}$ mice, for brevity) and Thy1.1^{+}/CD45.2^{+} WT B6 mice were infected with LCMV. After 30 days, 10^{7} lymphocytes, isolated from secondary lymphoid organs, were transferred into naive CD45.1^{+} B6 mice which were subsequently infected with LCMV. 40 days after infection, CD45.1^{+} mice were treated with tamoxifen to selectively ablate TCR from transferred Thy1.1^{-}/CD45.2^{+} TCRα$^{fl/fl}$ secondary memory T cells. **b, c,** LCMV-specific secondary memory T cells in peripheral blood are shown 40 days after LCMV infection (prior to tamoxifen treatment). Data pooled from three independent experiments for a total of $n = 8$ mice (**c**). **d**, **e**, Selective TCR ablation of TCRα$^{fl/fl}$ secondary memory CD8^{+} T cells as measured by ex vivo peptide stimulation assay. 60 days after tamoxifen treatment of CD45.1^{+} B6 recipients, splenocytes were isolated and stimulated in vitro with gp_{33-41} peptide. Cytokine production by TCR^{-} TCRα$^{fl/fl}$ memory CD8^{+} T cells and TCR^{+} WT

memory CD8$^+$ T cells from spleen is shown and reflects n = 6 mice (**d, e**). **f**, The frequency of cells that lack TCRβ expression on TCRα$^{fl/fl}$ memory CD8$^+$ T cells is shown. Data pooled from four independent experiments for a total of n = 8-10 mice (n varies by tissue) (**f**). **g**, Representative flow cytometry depicts expression of tissue-resident markers on small intestine epithelial (SI IEL) memory CD8$^+$ T cells 60 days after tamoxifen treatment. **h,** The frequency of CD69$^+$ memory CD8$^+$ T cells in the spleen is shown for WT and TCRβ$^-$ TCRα$^{fl/fl}$ populations. Data pooled from four independent experiments for a total of n = 8-10 mice (n varies by tissue) (**h**). Statistical significance was determined by two-tailed Wilcoxon matched-pairs signed rank test (**e, h**), where *p = 0.0313. Data are presented as mean values +/− SEM.

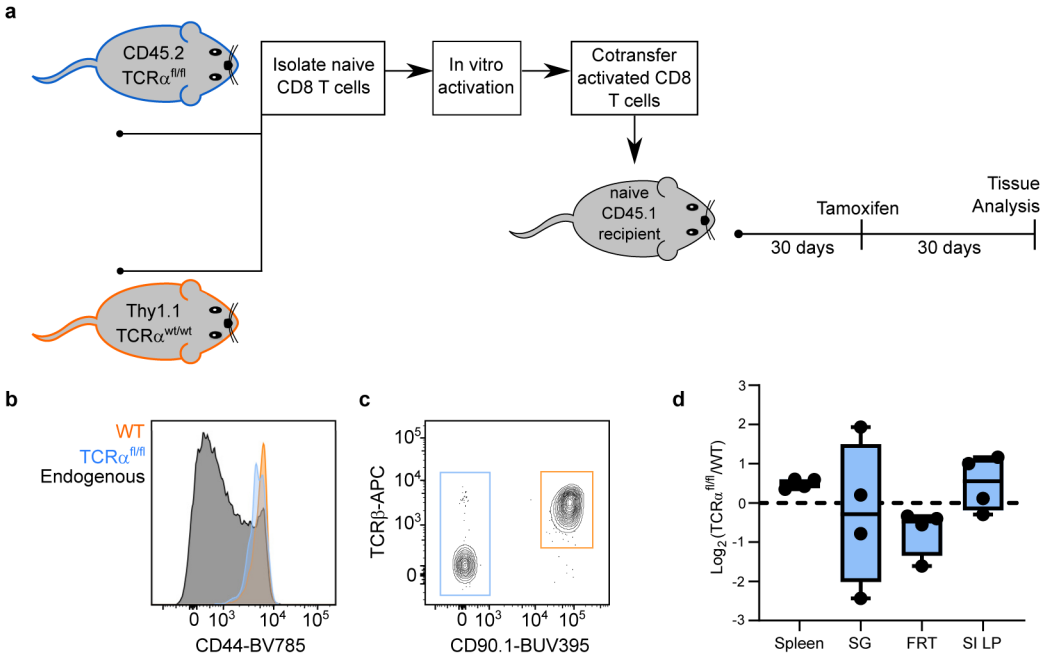

Extended Data Fig. 3. In vitro activation of TCRα$^{fl/fl}$ naïve T cells generates primary T$_{RM}$ that are maintained in the absence of constitutive TCR signaling.

a, Experimental model. Lymphocytes were isolated from secondary lymphoid organs of CD45.2$^+$ UBC-CreER^{T2} TCRα$^{fl/fl}$ mice (TCRα$^{fl/fl}$ mice, for brevity) and WT Thy1.1$^+$ B6 mice and enriched for naive CD8$^+$ T cells via magnetic bead enrichment. T cells were activated in vitro for 3 days with anti-CD3ε and rB7-1 and 10^7 cells were co-transferred into naïve CD45.1$^+$ B6 mice. 30 days later, recipients were treated with tamoxifen. 30 days after tamoxifen treatment, transferred CD8$^+$ T cells were evaluated for CD44 expression, as compared to endogenous CD8$^+$ T cells, shown via representative flow cytometry of CD8$^+$ T cells isolated from blood (**b**). Expression of TCRβ was evaluated for TCRα$^{fl/fl}$ and WT CD8$^+$ T cells, as shown via representative flow cytometry of peripheral blood (**c**). The ratio of TCRα$^{fl/fl}$/WT CD8$^+$ T cells was quantified 30 days after tamoxifen in various tissues, normalized to values from blood, and not significantly different from 1:1. (**d**). Data show n = 4 biologically independent mice from one experiment. Statistical significance was determined by two-tailed one sample Wilcoxon test using 0 as a hypothetical mean. Data are presented as box plots showing median, IQR, and extrema.

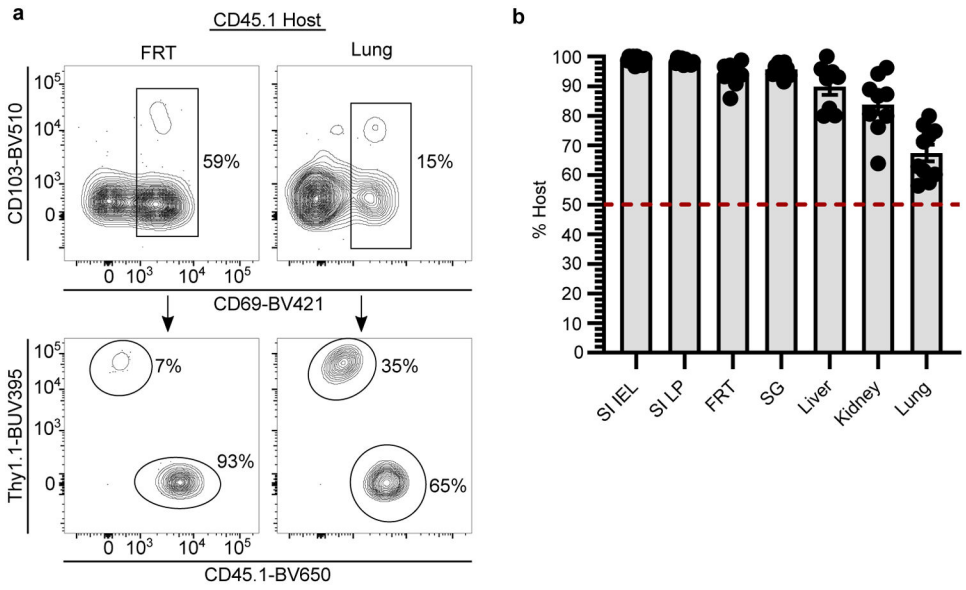

Extended Data Fig. 4. CD69 does not unequivocally distinguish long-lived resident memory T cells in the lung.

a-b, Representative flow cytometry (**a**) and graph (**b**) demonstrating degree of disequilibrium among CD69$^+$ extravascular memory P14 CD8$^+$ T cells in tissues of separated parabiotic mice (n = 10), 260 days after LCMV infection from one experiment. Upper panels are gated on extravascular memory CD8$^+$ P14 T cells (**a**). FRT, female reproductive tract. SI, small intestine. IEL, intestinal epithelial lymphocytes. LP, lamina propria. SG, salivary gland. Data are presented as mean values +/− SEM.

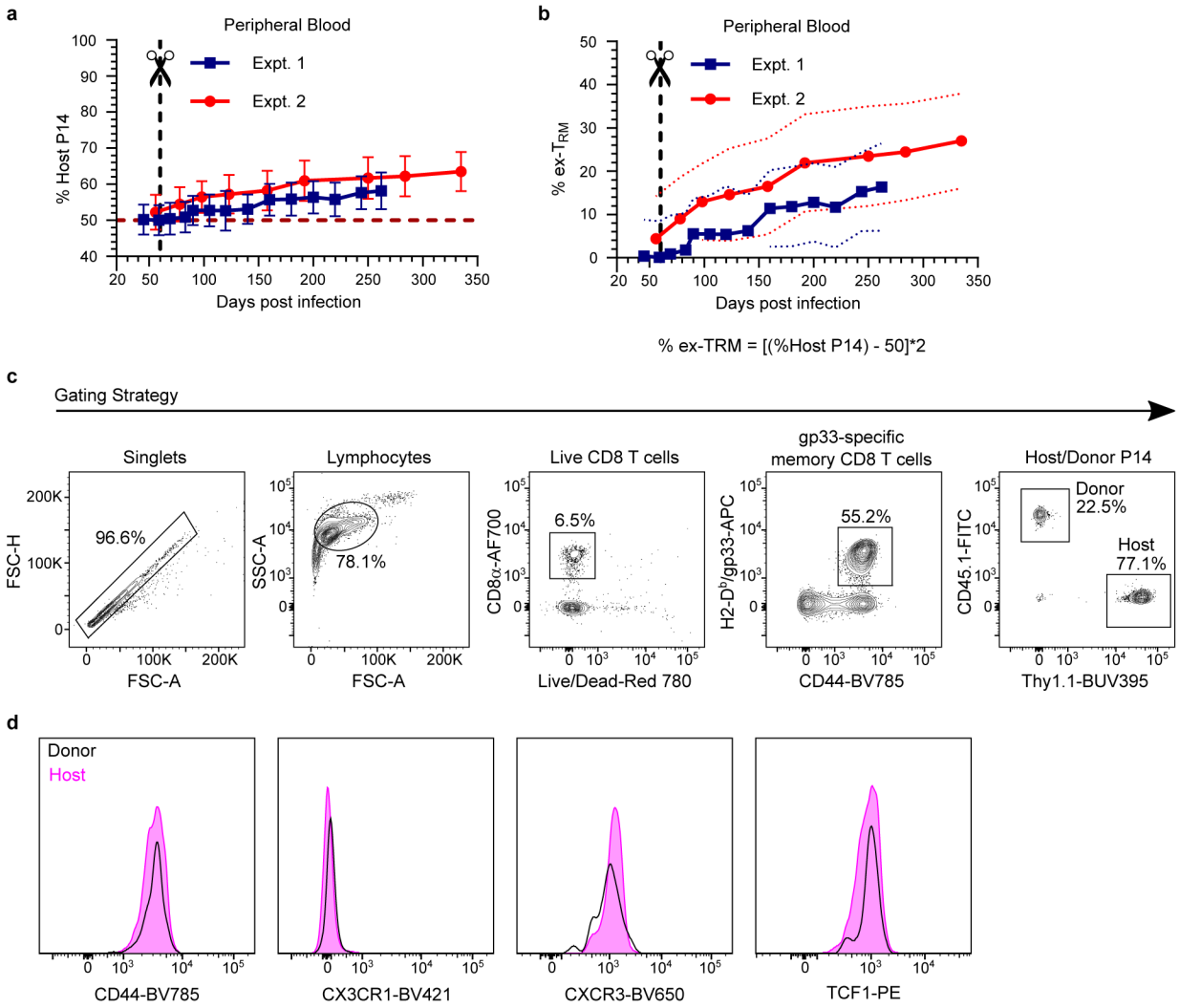

Extended Data Fig. 5. Ex-T_{RM} comprise a substantial fraction of bloodborne memory.

a-b, Longitudinal graphs depicting the frequency of host-derived memory P14 $CD8^+$ T cells (**a**) or the frequency of ex-T_{RM}, as calculated (**b**) in peripheral blood of separated parabiotic mice from two independent experiments ($n = 17$). Data are presented as mean values +/− SEM and in **b**, colored dotted lines reflect SEM (**b**). **c-d,** >200 days after separation of congenically distinct parabiotic P14 chimeras ($n = 17$), host- and donor-derived P14 $CD8^+$ T cells were evaluated for expression of markers of antigen experience, tissue-trafficking, and differentiation potential (**d**). Gating strategy for P14 $CD8^+$ T cells in separated parabiotic mice and generally representative of flow cytometry panels in Fig. 1, Fig. 2, Extended Data Fig. 2, Extended Data Fig. 3, Extended Data Fig. 4, and Extended Data Fig. 6 (**c**).

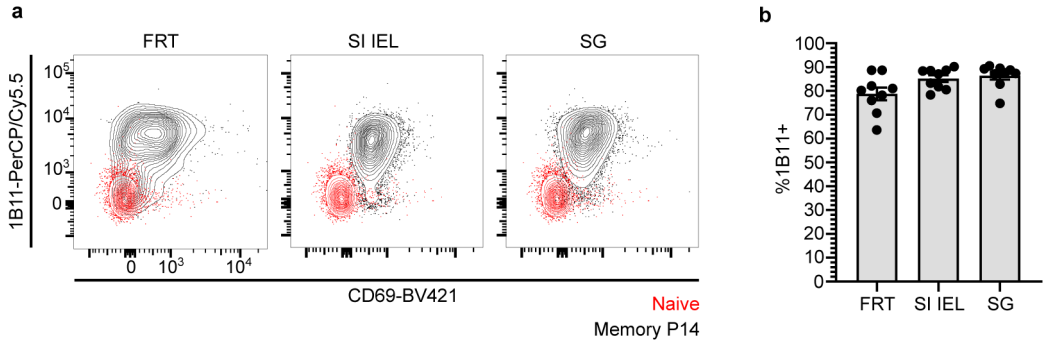

Extended Data Fig. 6. The 1B11-recognized glycoform of CD43 is expressed on resident memory CD8$^+$ T cells.

a, **b**, Representative flow cytometry (**a**) and quantification (**b**) of CD43-1B11 antibody staining on memory P14 CD8$^+$ T cells in nonlymphoid tissues of mice (n = 9) 200 days after LCMV. Naive CD8$^+$ T cells isolated from peripheral blood (in red) serve as basis for comparison (**a**). FRT, female reproductive tract. SI IEL, small intestinal epithelial lymphocytes. SG, salivary gland. Data are presented as mean values +/− SEM.

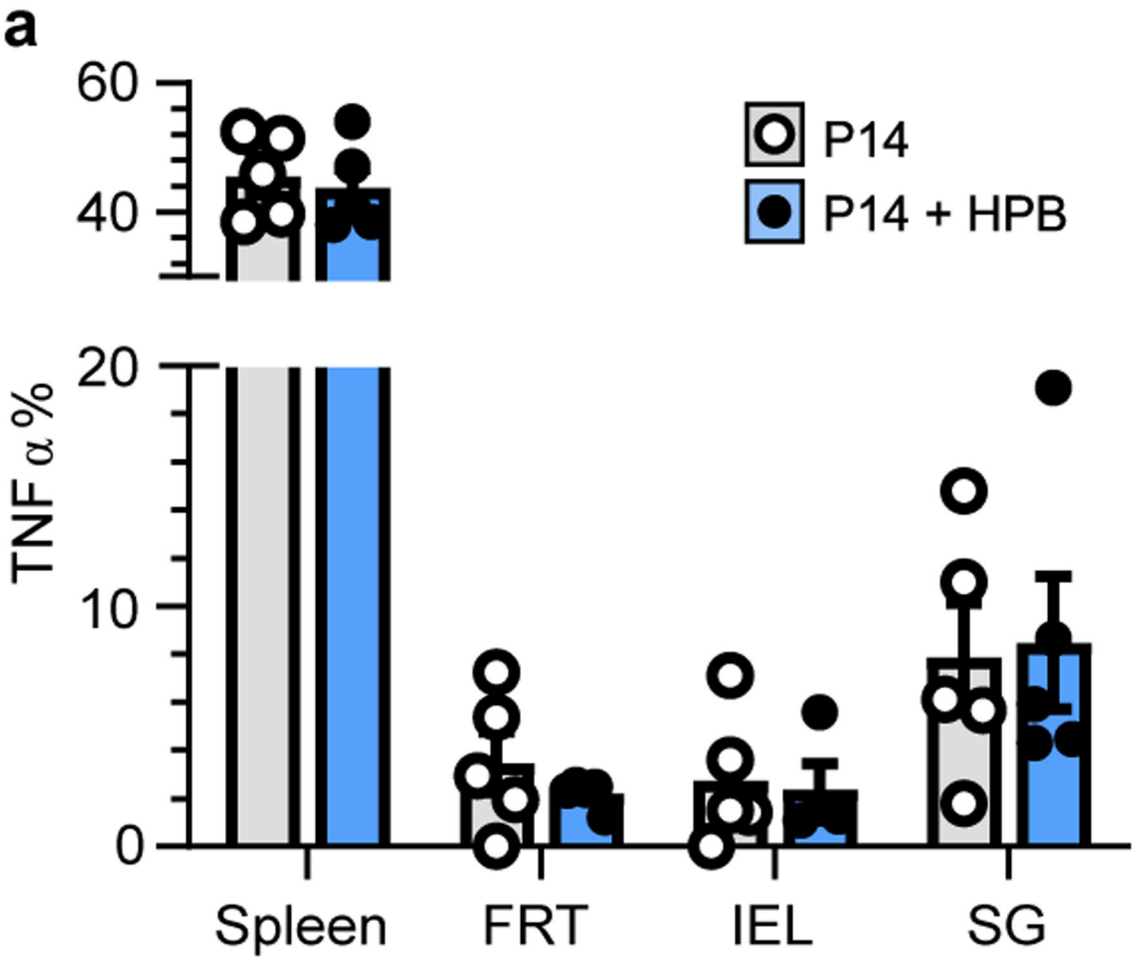

Extended Data Fig. 7. Preexisting memory T cells retain functional potency following heterologous prime-boost immunization.

a, 60 days after LCMV, P14 immune chimeras were subjected to heterologous prime-boost (HPB) regimen. Ex vivo functionality of memory P14 CD8$^+$ T cells in various tissues was compared and not statistically significant ($p > 0.05$) between $n = 4$-5 mice (n varies by tissue) receiving HPB and $n = 5$ age-matched control mice from one of two independent experiments with similar results. Statistical significance was determined by two-tailed Mann-Whitney U test. Data are presented as mean values +/− SEM.

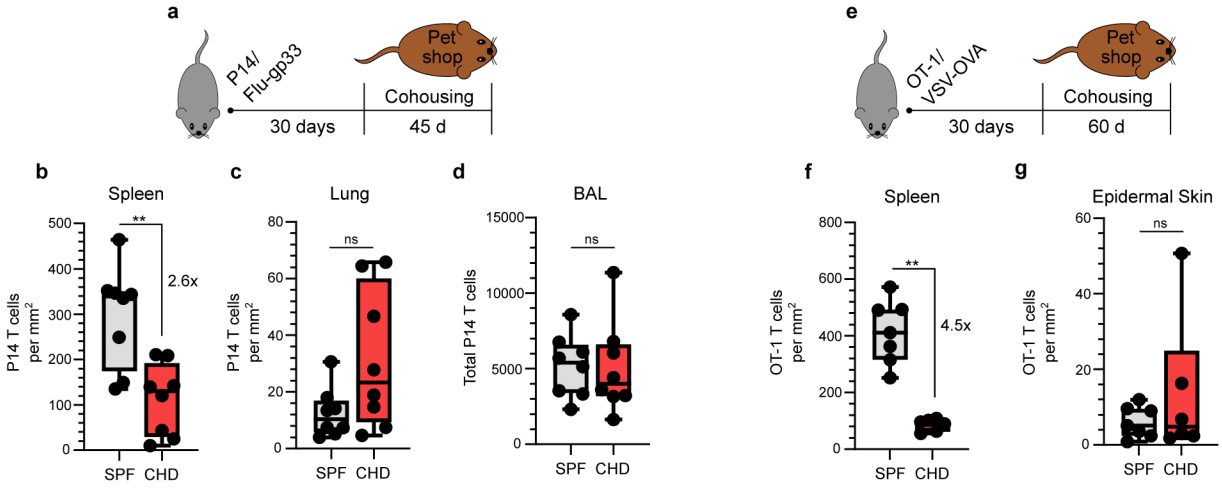

Extended Data Fig. 8. Lung or skin memory CD8$^+$ T cells are preserved following microbial experience.

a-d, P14 CD8$^+$ T cells were transferred into naïve mice, which were intranasally infected with PR8-gp33 influenza virus and 30 d later, mice were co-housed with pet shop mice for 45 d (**a**). P14 CD8$^+$ T cells from spleen (**b**), extravascular lung (**c**), and bronchoalveolar lavage (BAL) fluid (**d**) of co-housed mice ($n = 8$) were enumerated and compared to infection-matched mice housed in SPF conditions ($n = 8$) from one experiment. **e-g**, OT-1 CD8$^+$ T cells were transferred into naïve mice, which were intravenously infected with VSV-OVA and 30 d later, mice were co-housed with pet shop mice for 60 d (**e**). OT-1 CD8$^+$ T cells from spleen (**f**) and epidermal skin (**g**) of co-housed mice ($n = 6$) were enumerated and compared to infection-matched mice housed in SPF conditions ($n = 7$) from one experiment. Statistical significance was determined by two-tailed Mann-Whitney U test where $^{**}p = 0.0047$ (**b**) or $^{**}p = 0.0012$ (**f**). Data are presented as box plots showing median, IQR, and extrema.

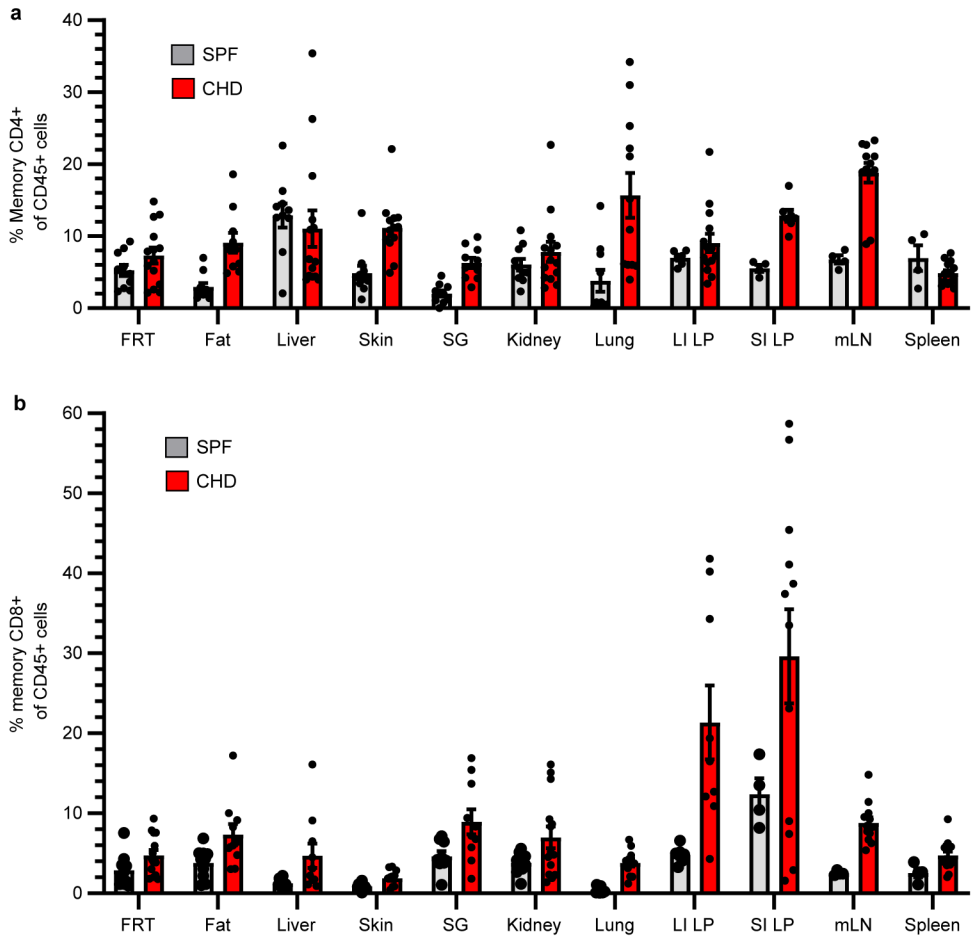

Extended Data Fig. 9. Both CD4$^+$ and CD8$^+$ memory T cell populations are expansible.

CD45$^+$ cells increase in tissues following co-housing (Fig. 3). Here we examined relative frequencies of memory T cells. **a**, **b**, C57Bl/6 SPF lab mice were co-housed with pet shop mice for >60 days. Age-matched conventionally housed SPF mice served as controls. The frequency of CD4$^+$ memory T cells (**a**) and CD8$^+$ memory T cells (**b**) as a proportion of CD45$^+$ immune cells is depicted in various tissues in both groups of mice. Memory T cells were defined as CD44$^+$/PD-1$^-$. mLN, mesenteric lymph node. Data pooled from two-four independent experiments for a total of n = 4-14 mice (n varies by tissue) per group. Data are presented as mean values +/− SEM.

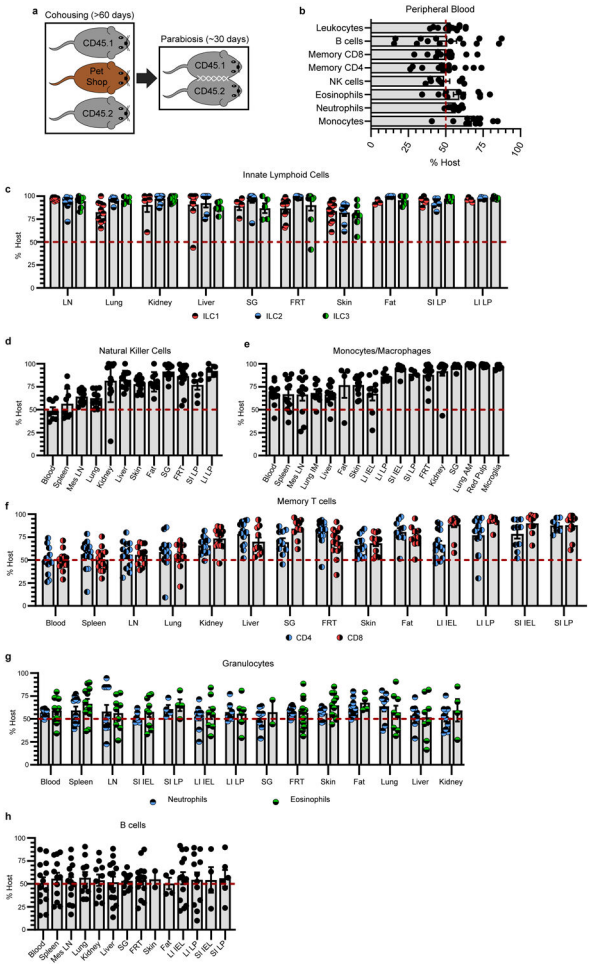

Extended Data Fig. 10. Tissue residence typifies immune surveillance for many cell types.

a, Model depicting co-housing CD45.1^{+} and CD45.2^{+} C57Bl/6 SPF lab mice with pet shop mice for >60 days followed by parabiosis of lab mice for 28-32 days. **b**, 28-32 days after parabiosis, equilibration of leukocyte populations in peripheral blood was evaluated in *n* = 8-14 mice. **c-h**, 28-32 days after parabiosis, tissue disequilibrium of innate lymphoid cells (**c**, *n* = 3-12 mice), natural killer cells (**d**, *n* = 5-14 mice), monocytes/macrophages (**e**, *n* = 4-12 mice), CD44^{+}/PD-1^{-} memory T cells (**f**, *n* = 7-14 mice), granulocytes (**g**, *n* = 4-12 mice) and B cells (**h**, *n* = 2-14 mice) was evaluated. Data pooled from four independent experiments and *n* varies dependent on tissue and population of interest, as not all cell populations were abundantly detected in each tissue or each experiment. IM, interstitial macrophages. AM, alveolar macrophages. Mes LN, mesenteric lymph node. Data are presented as mean values +/− SEM.

Acknowledgements

We thank members of the Masopust and Vezys laboratories for helpful discussions, Drs. Christoph Klose and David Artis for advice in identifying ILCs, University of Minnesota Flow Cytometry Resource, University Imaging Centers (Jason Mitchell, Thomas Pengo), and the Biosafety Level 3 Program. This study was supported by National Institutes of Health (NIH) grants R01 AI084913 (D.M.), F30 DK114942 and T32 AI007313 (S.W.), and the Howard Hughes Medical Institute Faculty Scholars program (D.M.).

References

1. Höfer T, Busch K, Klapproth K & Rodewald H-R Fate Mapping and Quantitation of Hematopoiesis In Vivo. Annu. Rev. Immunol 34, 449–478 (2016). [PubMed: 27168243]
2. Sawai CM et al. Hematopoietic Stem Cells Are the Major Source of Multilineage Hematopoiesis in Adult Animals. Immunity 45, 597–609 (2016). [PubMed: 27590115]
3. Janeway CA et al. Modes of cell:cell communication in the immune system. J. Immunol 135, 739s–742s (1985).
4. Qi H, Kastenmüller W & Germain RN Spatiotemporal basis of innate and adaptive immunity in secondary lymphoid tissue. Annu. Rev. Cell Dev. Biol 30, 141–67 (2014). [PubMed: 25150013]
5. Bromley SK et al. The immunological synapse. Annu. Rev. Immunol 19, 375–96 (2001). [PubMed: 11244041]
6. Mueller SN & Mackay LK Tissue-resident memory T cells: local specialists in immune defence. Nat. Rev. Immunol 16, 79–89 (2016). [PubMed: 26688350]
7. Szabo PA, Miron M & Farber DL Location, location, location: Tissue resident memory T cells in mice and humans. Sci. Immunol 4, 1–12 (2019).
8. Steinert EM et al. Quantifying Memory CD8 T Cells Reveals Regionalization of Immunosurveillance. Cell 161, 737–49 (2015). [PubMed: 25957682]
9. Stark R et al. T_{RM} maintenance is regulated by tissue damage via P2RX7. Sci. Immunol 3, eaau1022 (2018). [PubMed: 30552101]
10. Murali-Krishna K et al. Persistence of memory CD8 T cells in MHC class I-deficient mice. Science 286, 1377–81 (1999). [PubMed: 10558996]
11. Masopust D, Vezys V, Wherry EJ, Barber DL & Ahmed R Cutting edge: gut microenvironment promotes differentiation of a unique memory CD8 T cell population. J. Immunol 176, 2079–83 (2006). [PubMed: 16455963]
12. Kurd NS et al. Early precursors and molecular determinants of tissue-resident memory CD8+ T lymphocytes revealed by single-cell RNA sequencing. Sci. Immunol 5, eaaz6894 (2020). [PubMed: 32414833]
13. Sallusto F, Geginat J & Lanzavecchia A Central memory and effector memory T cell subsets: function, generation, and maintenance. Annu. Rev. Immunol 22, 745–63 (2004). [PubMed: 15032595]
14. Germain RN & Huang Y ILC2s - resident lymphocytes pre-adapted to a specific tissue or migratory effectors that adapt to where they move? Curr. Opin. Immunol 56, 76–81 (2019). [PubMed: 30472437]
15. Klicznik MM et al. Human CD4+CD103+ cutaneous resident memory T cells are found in the circulation of healthy individuals. Sci. Immunol 4, eaav8995 (2019). [PubMed: 31278120]
16. Carbone FR & Gebhardt T Should I stay or should I go-Reconciling clashing perspectives on CD4+ tissue-resident memory T cells. Sci. Immunol 4, 8–10 (2019).
17. Wu T et al. Lung-resident memory CD8 T cells (T_{RM}) are indispensable for optimal cross-protection against pulmonary virus infection. J. Leukoc. Biol 95, 215–24 (2014). [PubMed: 24006506]
18. Slütter B et al. Dynamics of influenza-induced lung-resident memory T cells underlie waning heterosubtypic immunity. Sci. Immunol 2, (2017).
19. Stockinger B, Barthlott T & Kassiotis G The concept of space and competition in immune regulation. Immunology 111, 241–247 (2004). [PubMed: 15009422]
20. Surh CD & Sprent J Homeostasis of Naive and Memory T Cells. Immunity 29, 848–862 (2008). [PubMed: 19100699]
21. Buck MD, Sowell RT, Kaech SM & Pearce EL Metabolic Instruction of Immunity. Cell 169, 570–586 (2017). [PubMed: 28475890]
22. Schenkel JM et al. IL-15–Independent Maintenance of Tissue-Resident and Boosted Effector Memory CD8 T Cells. J. Immunol 196, 3920–3926 (2016). [PubMed: 27001957]
23. Vezys V et al. Memory CD8 T-cell compartment grows in size with immunological experience. Nature 457, 196–199 (2009). [PubMed: 19005468]

24. Huster KM et al. Cutting edge: memory CD8 T cell compartment grows in size with immunological experience but nevertheless can lose function. J. Immunol 183, 6898–902 (2009). [PubMed: 19890045]
25. Beura LK et al. Normalizing the environment recapitulates adult human immune traits in laboratory mice. Nature 532, 512–6 (2016). [PubMed: 27096360]
26. Gasteiger G, Fan X, Dikiy S, Lee SY & Rudensky AY Tissue residency of innate lymphoid cells in lymphoid and nonlymphoid organs. Science (80-.). 350, 981–985 (2015).
27. Guilliams M, Thierry GR, Bonnardel J & Bajenoff M Establishment and Maintenance of the Macrophage Niche. Immunity 52, 434–451 (2020). [PubMed: 32187515]
28. Schmidt-Rhaesa A The evolution of organ systems. (Oxford University Press, 2007).
29. Pabst O, Herbrand H, Bernhardt G & Förster R Elucidating the functional anatomy of secondary lymphoid organs. Curr. Opin. Immunol 16, 394–399 (2004). [PubMed: 15245731]
30. van Furth R & Cohn ZA The origin and kinetics of mononuclear phagocytes. J. Exp. Med 128, 415–435 (1968). [PubMed: 5666958]
31. Sallusto F, Lenig D, Förster R, Lipp M & Lanzavecchia A Two subsets of memory T lymphocytes with distinct homing potentials and effector functions. Nature 401, 708–12 (1999). [PubMed: 10537110]
32. Weissman IL Stem cells: units of development, units of regeneration, and units in evolution. Cell 100, 157–68 (2000). [PubMed: 10647940]
33. Gattinoni L, Speiser DE, Lichterfeld M & Bonini C T memory stem cells in health and disease. Nat. Med 23, 18–27 (2017). [PubMed: 28060797]
34. Iwasaki A Exploiting Mucosal Immunity for Antiviral Vaccines. Annu. Rev. Immunol 34, 575–608 (2016). [PubMed: 27168245]
35. Amsen D, van Gisbergen KPJM, Hombrink P & van Lier RAW Tissue-resident memory T cells at the center of immunity to solid tumors. Nat. Immunol 19, 538–546 (2018). [PubMed: 29777219]
36. Fonseca R et al. Developmental plasticity allows outside-in immune responses by resident memory T cells. Nat. Immunol 21, 412–421 (2020). [PubMed: 32066954]
37. Behr FM et al. Tissue-resident memory CD8+ T cells shape local and systemic secondary T cell responses. Nat. Immunol 21, 1070–1081 (2020). [PubMed: 32661361]

Methods References

38. Polic B, Kunkel D, Scheffold A & Rajewsky K How alpha beta T cells deal with induced TCR alpha ablation. Proc. Natl. Acad. Sci. U. S. A 98, 8744–9 (2001). [PubMed: 11447257]
39. Ruzankina Y et al. Deletion of the Developmentally Essential Gene ATR in Adult Mice Leads to Age-Related Phenotypes and Stem Cell Loss. Cell Stem Cell 1, 113–126 (2007). [PubMed: 18371340]
40. Tucker CG et al. Adoptive T Cell Therapy with IL-12–Preconditioned Low-Avidity T Cells Prevents Exhaustion and Results in Enhanced T Cell Activation, Enhanced Tumor Clearance, and Decreased Risk for Autoimmunity. J. Immunol 205, 1449–1460 (2020). [PubMed: 32737148]
41. Schindelin J et al. Fiji: an open-source platform for biological-image analysis. Nat. Methods 9, 676–82 (2012). [PubMed: 22743772]
42. Anderson KG et al. Intravascular staining for discrimination of vascular and tissue leukocytes. Nat. Protoc 9, 209–22 (2014). [PubMed: 24385150]
43. Klose CSN et al. The neuropeptide neuromedin U stimulates innate lymphoid cells and type 2 inflammation. Nature 549, 282–286 (2017). [PubMed: 28869965]
44. Guilliams M et al. Unsupervised High-Dimensional Analysis Aligns Dendritic Cells across Tissues and Species. Immunity 45, 669–684 (2016). [PubMed: 27637149]
45. Jiang X et al. Skin infection generates non-migratory memory CD8+ T(RM) cells providing global skin immunity. Nature 483, 227–31 (2012). [PubMed: 22388819]

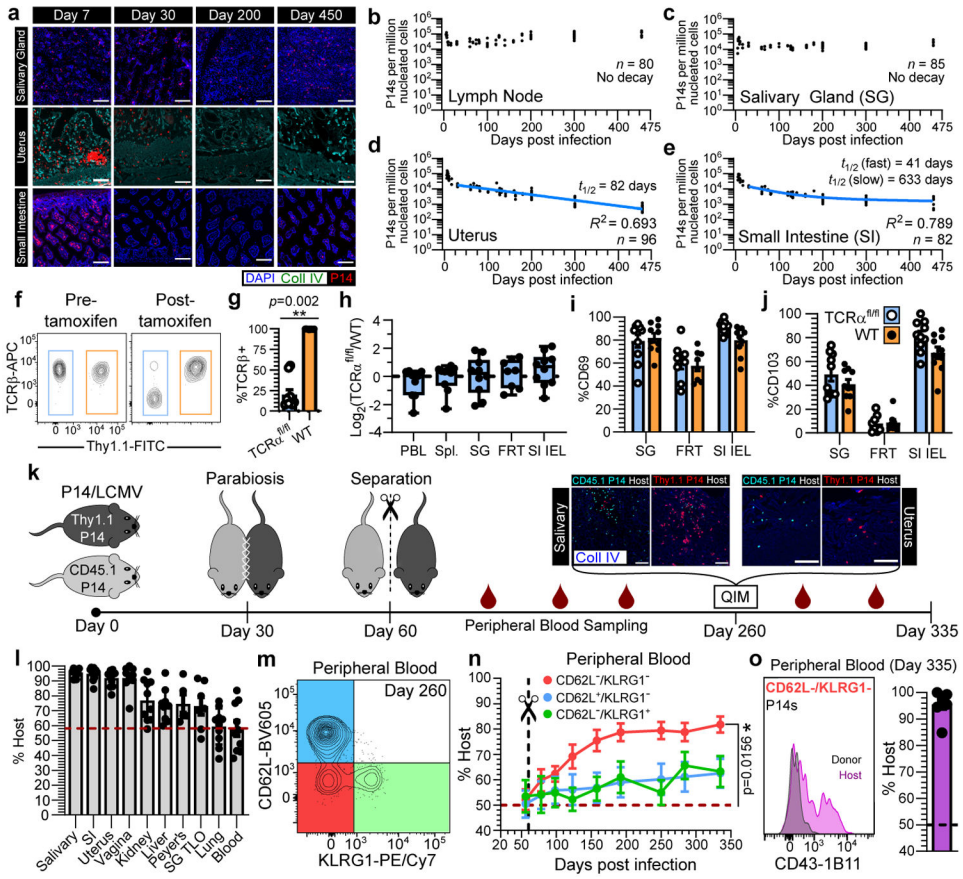

Fig. 1. Residence sustains organism-wide autonomous T cell immune surveillance.

a-e, Using quantitative immunofluorescent microscopy (QIM) (**a**), P14 memory CD8$^+$ T cells were enumerated five to 450 days after LCMV infection in n = 80-96 biologically independent mice from six independent experiments (**b-e**). **f-j,** Secondary LCMV-specific TCRα$^{fl/fl}$ and WT memory T cells were established (see methods and Extended Data Fig. 2a) and mice were treated with tamoxifen to selectively ablate TCR, as evaluated 12 days post-treatment (**f, g**). To assess the impact of TCR ablation on T cell survival, the ratio of TCRα$^{fl/fl}$/WT CD8$^+$ T cells was quantified 60 days after tamoxifen and normalized to pre-tamoxifen values from blood (**h**). Expression of residence markers was compared between WT and TCRβ$^-$ TCRα$^{fl/fl}$ T_{RM} (**i, j**). Data pooled from four independent experiments for a total of n = 10 mice, except FRT, n = 8 mice (**g-j**). **k-o,** Congenically distinct parabiotic P14 chimeras were surgically separated **(k)** and 260 days after LCMV, n = 5-10 mice (n varies by tissue) were examined by QIM to evaluate durability of residence among extravascular P14 memory CD8$^+$ T cells (**l**). After separation, peripheral blood of n = 7 parabiotic P14 chimera mice was serially monitored for reemergence of disequilibrium among P14 memory CD8$^+$ T cells, which were subdivided based on CD62L/KLRG1 expression (**m, n**) and 335 days after LCMV, CD62L$^-$/KLRG1$^-$ donor and host P14 memory CD8$^+$ T cells were evaluated for CD43-1B11 (**o**). Coll IV, collagen type IV. FRT, female reproductive tract. IEL, intestinal epithelial lymphocytes. TLO, tertiary lymphoid organ. 100 μm scale bars (**a, k**). Statistical significance was determined by two-tailed Wilcoxon matched-pairs signed rank test (**g, i, j**) and two-tailed one sample Wilcoxon test using 0 (**h**) or 50% (**n**) as a hypothetical mean.

Data are presented as mean values +/− SEM or box plots showing median, IQR, and extrema.

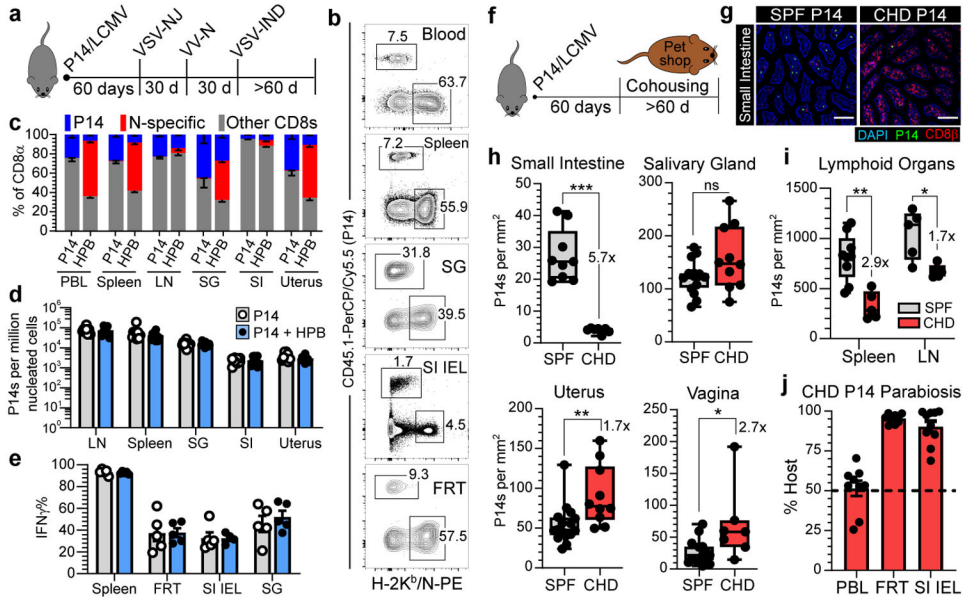

Fig. 2. The CD8$^+$ T cell compartment expands to accommodate new and preexisting resident memory.

a-e, 60 days after LCMV, P14 immune chimeras were subjected to heterologous prime-boost (HPB) to generate a robust CD8$^+$ T cell response against the nucleoprotein (N) epitope of VSV (**a, b**). Numerical abundancy, evaluated by flow cytometry (**c**) and QIM (**d**), and ex vivo functionality (**e**) of memory P14 CD8$^+$ T cells in various tissues was compared and not statistically significant ($p > 0.05$) (**d, e**) between mice receiving HPB and age-matched control mice. Data shown from one of two independent experiments with similar results with $n = 4$-5 mice per group, per experiment (**c, e**). Data pooled from two independent experiments for a total of $n = 8$-10 mice per group (**d**). **f-i,** 60 days after LCMV, P14 immune chimeras were co-housed with pet shop mice to facilitate microbial exposure. Memory P14 CD8$^+$ T cells in nonlymphoid ($n = 7$-10, 16 mice) (**h**) and lymphoid ($n = 5$,9 mice) **(i)** tissues were enumerated by QIM in two independent experiments (**h, i**). **j,** P14 chimeras were co-housed with pet shop mice for >60 days, conjoined via parabiosis for 30 days, at which point disequilibrium of memory P14 CD8$^+$ T cells was assessed in $n = 9$-10 mice. LN, lymph node. 100 μm scale bars (**g**). Statistical significance was determined by two-tailed Mann-Whitney U test where *$p = 0.0172$, **$p = 0.0028$, ***$p = 0.0002$ (**h**) or *$p = 0.0159$, **$p = 0.0040$ (**i**). Data are presented as mean values +/− SEM or box plots showing median, IQR, and extrema.

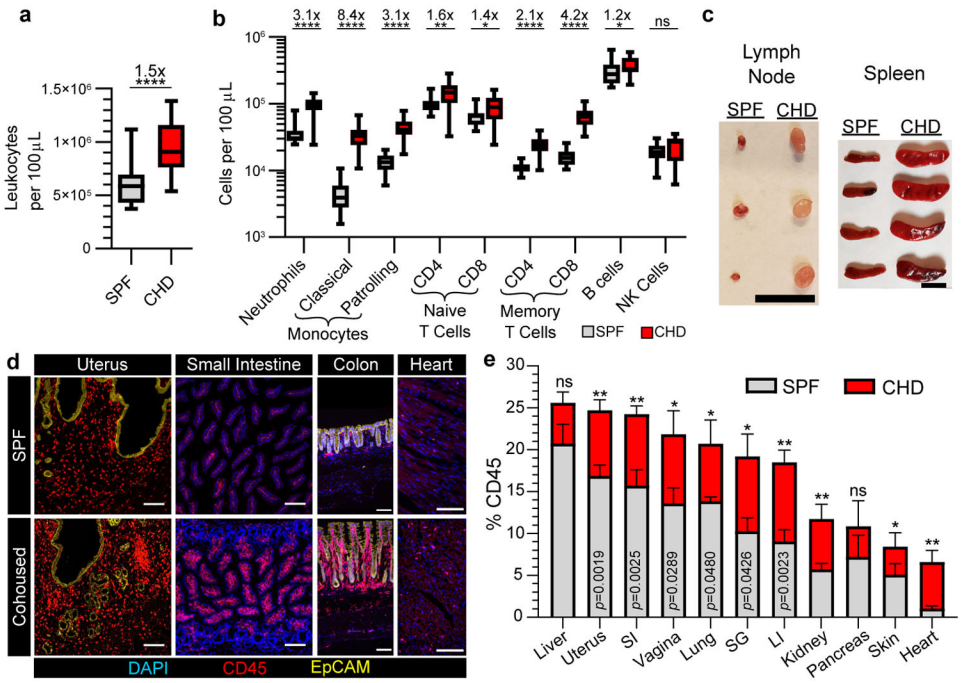

Fig. 3. Tissue pliancy allows for immune expansion following microbial conditioning.

a, b, The abundance of total leukocytes (**a**) and immune subpopulations (**b**) in peripheral blood was compared between $n = 21$ B6 mice co-housed (CHD) with pet shop mice for 90 days and $n = 21$ B6 mice housed in conventional SPF conditions. **c,** Representative lymphoid organs from SPF and CHD mice. **d, e,** The frequency of immune cells contributing to total organ cellularity (quantified by enumeration of total nucleated cells) in SPF and CHD mice was evaluated by QIM. CHD mice were co-housed for 90-120 days (**c-e**). Data pooled from four independent experiments, $n = 5$-16 mice per group, except pancreas $n = 3$-5 mice (**d, e**). LI, large intestine. 1 cm scale bar (**c**), 100 µm scale bars (**d**). EpCAM staining shown for uterus and colon only; DAPI staining excluded for uterus (**d**). Statistical significance was determined by two-tailed Mann-Whitney U test where $*p = 0.0209$ (naïve CD8), $*p = 0.0336$ (B cells), $**p = 0.0022$, $****p < 0.0001$ (**a, b**), or $*p = 0.0418$, $**p = 0.0047$ (kidney), $**p = 0.0043$ (heart) or as shown in graph (**e**). Data are presented as mean values +/− SEM or box plots showing median, IQR, and extrema.

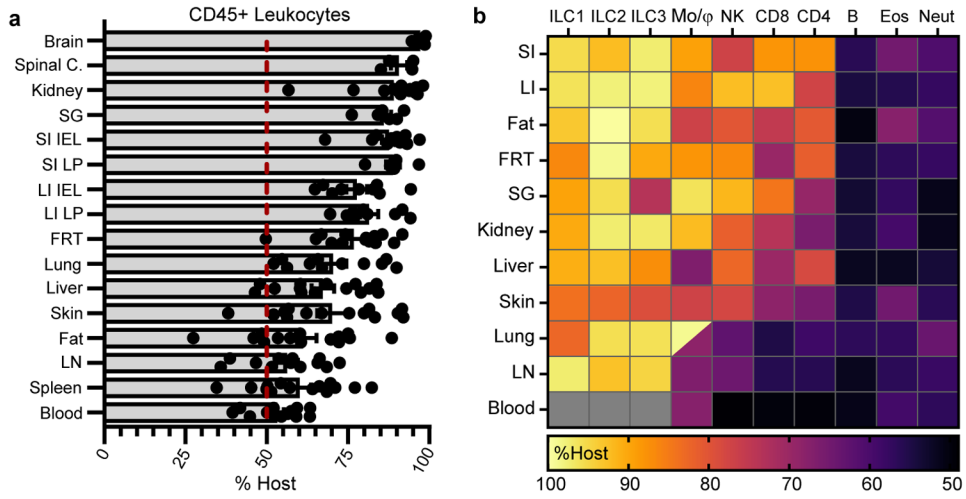

Fig. 4. Tissue residence typifies organism-wide immune surveillance.

a, b, Congenically distinct B6 mice were co-housed with pet shop mice. After >60 days, mice were conjoined by parabiosis for 28-32 days. Equilibration of total leukocytes (**a**) and immune populations (**b**) was evaluated in peripheral blood and tissues. Lung and kidney populations exclude intravascular leukocytes. In heatmap (**b**), lung macrophages are divided into alveolar (top left) and interstitial (bottom right) populations, intestinal populations were isolated from lamina propria (LP), and gray denotes populations that were not detectable. Heatmap shows mean percentage value of host-derived cells. Data pooled from four independent experiments. Typically, n = 8-14 mice, with exceptions for some tissues or cell types (see Extended Data Fig. 10) (**a**, **b**). ILC, innate lymphoid cells. Mo/Mϕ, monocytes/macrophages. NK, natural killer cells. CD4/CD8 refers to memory T cells ($CD44^{+}/PD\text{-}1^{-}$). B, B cells. Eos, eosinophils. Neut, neutrophils. Data are presented as mean values +/− SEM.